Competition between electroosmotic and chemioosmotic flow in charged nanofluidics

Sourayon Chanda and Peichun Amy Tsai*
Department of Mechanical Engineering, University of Alberta, Edmonton, Alberta T6G 2G8, Canada.
(Dated: December 26, 2020)

In electrolyte solutions, charged nanoscale pores or channels with overlapping electrical double layers are charge selective, thereby benefiting a wide range of applications such as desalination, bio-sensing, membrane technology, and renewable energy. As an important forcing mechanism, a gradient of electrolyte concentration along a charged nano-confinement can drive flow without an external electrical field or applied pressure difference. In this paper, we numerically investigate such diffusioosmotic nanoflow, particularly for dilute electrolyte concentrations (of $0.01-1$ mM), and calculate the corresponding electrical and concentration fields in a charged nanochannel connecting two reservoirs of different salt concentrations—a typical fluidic configuration for a variety of experimental applications. Under a wide range of parameters, the simulation results show that the flow speed inside the nanochannel is linearly dependent on the concentration difference between the two reservoir solutions, Δc, whereas the flow direction is primarily influenced by three key parameters: nanochannel length (l), height (h), and surface charge density (σ). Through a comparison of the chemioosmotic (due to ion-concentration difference) and electroosmotic (as a result of the induced electric field) components of this diffusioosmotic flow, a non-dimensional number ($C = h/\sqrt{l\lambda_{GC}}$) has been identified to delineate different nanoscale flow directions in the charged nanochannel, where λ_{GC} is a characteristic (so-called Gouy-Chapman) length associated with surface charge and inversely proportional to σ. This critical dimensionless parameter, dependent on the above three key nanochannel parameters, can help in providing a feasible strategy for flow control in a charged nanochannel.

I. INTRODUCTION

Nanofluidic transport has lately attracted significant interest due to the advent of nanofabrication [1–3] as well as its beneficial surface-dominant (or induced) effects [4–7]. For instance, nano-slits (typically of the order of 10 – 100 nm) can become charge-selective due to overlapping electrical double layers (EDLs) in an electrolyte solution and, hence, allow electrical interaction and manipulation [8–10]. This underlying mechanism has recently been applied to various promising applications of nanofluidics for desalination [11–14], membrane technology [8, 15], cell biology [2, 16], and sustainable energy using reverse electrodialysis [17–21].

Nanoflow generally can be driven or manipulated by several external forcing mechanisms, such as, via temperature difference [22, 23], capillary action [24, 25] or external electrical field [7, 26, 27]. For example, the electroosmotic flow (EOF) with an external electrical field is commonly used and affected by the induced ion distribution within the EDLs along a charged surface [28]. Less attention, however, has been given to the flow generated across a charged nano-confinement under an electrolyte concentration gradient [29–31]. This so-called diffusioosmotic flow (DOF) is a combination of two effects: namely, chemiosmosis and electroosmosis. Chemiosmotic flow is fluid motion due to diffusion under an electrolyte concentration gradient, which induces a pressure gradient along the charged surface [32–34]. Whereas, the motion due to the electrical interactions between spatial charges and the electrical field induced within the double layers is termed as electroosmosis [35–38].

Most previous analytical studies of diffusioosmosis considered an electrolyte solution subjected to a concentration gradient along a homogeneously-charged surface, using simplified, 1D Poisson-Boltzmann distribution of electrolyte concentration [32, 33, 39–43]. Keh et al. reported a closed form expression of diffusioosmotic velocity of the electrolyte by a force balance at equilibrium [32]. In the limit of small zeta potential or surface charge density at the wall, Keh et al. found a monotonic increase of diffusioosmotic flow with increasing zeta potential [32]. Keh et al. further demonstrated the non-linear increase of diffusioosmotic velocity with decreasing porosity in a charged porous medium with a 1D formulation of diffusioosmotic velocity as a function of EDL thickness, ion diffusivities, and pore diameter [33, 41].

Motivated by bio-medical and bio-sensing applications exploiting ion concentration polarization (ICP) with distinct ion-depletion and ion-enrichment zones [14, 27, 44, 45] in nano-confinements, recent numerical investigations consider 2D configuration of micro-nano junctions to investigate DOF [34, 46, 47]. These studies of 2D DOF problem reveal a significant dependence of diffusioosmotic velocity on surface charge, concentration gradient, and dimensions of the nano-confinement. More specifically, diffusioosmotic velocity was found to increase with increasing surface charge density [46] and increasing nanochannel aspect ratio [34], but depend nonlinearly on electrolyte concentration [46, 47].

Intriguingly, the reversal of diffusioosmotic flow was found with a small zeta potential of planar charged

* peichun.amy.tsai@ualberta.ca

nanochannel [32, 41], at a low electrolyte concentration [46] or by tuning width-to-height ratio [34]. One numerical study reported that DOF in a negatively-charged (of -20×10^{-3} C/m^2) nanopore (of a radius of $4 - 12$ nm and length of 80 nm) occurs in the direction from the adjacent, high-concentration reservoir to low-concentration one [47]. Despite insightful findings by these investigations considering a planar or homogeneous flow geometry, common experimental setups involving nano/micro-junctions [48–53] are quasi-2D or 3D problems of single or several nano-slit connecting micro-channels (See Fig. 1, for example) and are hardly considered theoretically or numerically due to the complexity of the flow geometry.

In addition, recent experiments using nano/micro-junction systems have shown several intriguing and exciting findings, for example, continuous stream of direct seawater desalination [11], experimental water flow rate (of femtoliters per minute) attributed to DOF inside nanochannels [54], experimental nanoflow direction under a concentration gradient of neutral solutes using a fluorescent dye [55] as well as promising applications of desalination [11, 13, 14], water purification [56, 57], nanofluidic diodes [58–60] and energy harvesting with a salinity gradient [18, 19, 61], but mostly lack direct measurements of local flow and electrical fields. To fill these literature gaps, specifically regarding a better understanding of local fields and feasible manipulation of diffusioosmotic nanoflow, we numerically investigate DOF in a charged nanochannel without any external electrical forcing.

Our numerical model consists of a central, charged nanochannel connected to two reservoirs with external solutions of different concentrations, as a fundamental working element of typical nano/micro-junctions. Local electrical, ion-concentration and flow fields are computed. The results under various concentrations show a linear dependence of the DOF magnitude on the external concentration gradient. Moreover, the numerical results suggest a critical characteristic dimensionless number (C^*) that conveniently delineates the parameter regions into different DOF directions for various channel dimensions and surface charge. We further carry out scaling analyses to explain the underlying mechanisms associated with C^*, which is the ratio of chemiosmotic to electroosmotic velocity. We show a feasible control of DOF flow by tuning h, l, and σ, i.e., through C, so that chemiosmosis (for $C > C^*$) or electroosmosis (for $C < C^*$) dominates the DOF flow and, hence, governs the nanoflow direction.

II. MATHEMATICAL MODELING

We numerically compute the flow, electrical, and ion concentration fields of a 2D steady-state diffusioosmosis problem, where two steady-flow reservoirs of different electrolyte concentrations (of KCl) are connected by a nanochannel with a constant (positive) surface charge density, σ (see Fig. 1). A steady flux of electrolyte solution of high concentration (c_H) is injected through one

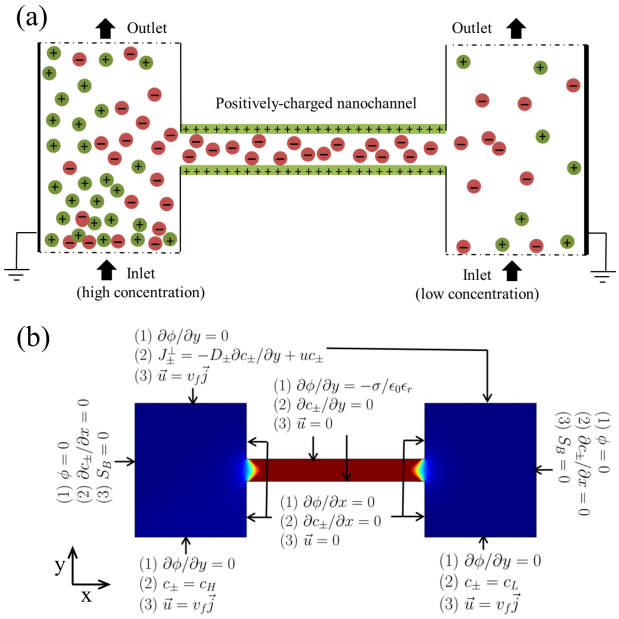

FIG. 1. (a) Schematic of the simulation model of a 2D steady-sate diffusioosmotic flow through a charge-selective nanochannel connecting two reservoirs of different electrolyte concentrations; (b) the boundary conditions used for simulating the diffusioosmotic flow through a charge selective nanochannel of height (h) and length (l). In (b), the number corresponds to the Eq. number described in the mathematical model (Section II).

reservoir (on the left), while a low concentration (c_L) through the other (on the right). Interaction between the two different solutions via the nanochannel is significantly affected by the nanochannel surface charge, resultant electric double layer, and concentration difference, $\Delta c = c_H - c_L$. The thickness of EDL can be characterized by the Debye length, λ_D. For a symmetric monovalent ($z_+ = -z_- = z = 1$) electrolyte, λ_D can be estimated by $\lambda_D = \sqrt{\epsilon_0\epsilon_r RT/2F^2 c_0}$, where c_0 is the molar concentration of the electrolyte solution [62]. Typical λ_D of our system varies between 10 nm (for $c_0 \approx 1$ mM) and 100 nm (for $c_0 \approx 0.01$ mM), estimated using the average electrolyte concentration in the nanochannel.

Narrow nanochannel with overlapping EDL causes the nanochannel to be charge selective due to the repulsion of co-ions and attraction of counter-ions by the charged wall. This charge selectivity is, however, diminished for wider channel due to insufficient screening of the co-ions. Simultaneously, a concentration gradient across the nanochannel due to the difference in electrolyte concentration drives the chemiosmotic transport of the electrolyte solutions. Due to the complex interplay of these different phenomena, it is fascinating and useful to numerically study diffusioosmotic flow in micro-nano junctions based on the conservation of mass, momentum, species, and charges.

The distribution of electric potential, ϕ, is governed by

the Poisson equation due to spatial net charges [63]:

$$\epsilon_0\epsilon_r\nabla^2\phi = -F(z_+c_+ + z_-c_-), \quad (1)$$

where ϵ_0 (= 8.854×10^{-12} Fm^{-1}), ϵ_r (= 80.1) and F (= 96485 C mol^{-1}) are the permittivity of a vacuum, relative permittivity of water, and Faraday constant, respectively. c_+ and z_+ (= +1 for K^+ ion) are the concentration and valence of the cation, whereas c_- and z_- (= -1 for Cl^- ion) are the concentration and valence of the anion.

The ion concentrations in the solution (i.e., c_+ or c_- for the cation and anion, respectively) are governed by the conservation of ionic species or fluxes and described by the Nernst-Planck equations.[64] Considering a steady problem, these equations for c_+ and c_- can be modeled using the concept of conservation of ionic fluxes, $J_\pm$ [64, 65]:

$$\nabla \cdot J_\pm = -\vec{\nabla} \cdot (D_\pm\vec{\nabla}c_\pm + \frac{D_\pm}{RT}z_\pm F c_\pm \vec{\nabla}\phi) + \vec{u}\cdot\vec{\nabla}c_\pm = 0, \quad (2)$$

where T (= 293 K) is the operating temperature, R (= 8.314 JK^{-1}mol^{-1}) is the universal gas constant, and D_+ and D_- are the diffusivities of the cation and anion, respectively.

Corresponding to the diffusivities of K^+ and Cl^- ions, D_+ and D_- are assumed to be 1.96×10^{-9} m^2/s and 2.0×10^{-9} m^2/s. Physically, the governing Eq. (2) describes the conservation of ionic species via diffusive, electromigration, and convective ion-fluxes due to the presence of concentration gradient, electrical forcing, and fluid velocity, respectively, which are represented by the each sequential terms in Eq. (2) [28, 64]. The competition among these factors dictates the ionic flux inside the nano-confinement. Integrating Eq. (2), we can obtain the cationic (J_+) or anionic (J_-) fluxes. The mathematical expression of J_+ or J_- is given by

$$\vec{J_\pm} = (-D_\pm\vec{\nabla}c_\pm - \frac{z_\pm D_\pm F c_\pm}{RT}\vec{\nabla}\phi) + \vec{u}c_\pm. \quad (3)$$

The flow field, $\vec{u}$, is simulated by solving the steady-state Navier-Stokes equations [64, 66], along with the Continuity equation. The Navier-Stokes equations are simplified to the Stokes equations due to the negligible effect of inertia at a low Reynolds number flow (here, our $Re \approx 10^{-5}$ for l = 100 nm and v_f = 0.01 mm/s):

$$\nabla \cdot \vec{u} = 0, \quad (4)$$

$$-\vec{\nabla}p + \mu\nabla^2\vec{u}\underbrace{-F(z_+c_+ + z_-c_-)\vec{\nabla}\phi}_{\vec{F_e}=q\vec{E}=-q\vec{\nabla}\phi} = 0, \quad (5)$$

where μ is the liquid viscosity (for water, $\mu \simeq 1$ mPa·s at room temperature), $\vec{F_e}$ is the electrical body force, and q ($= z_+c_+ + z_-c_-$) is the net charge. Eq. sets (1)–(5) are non-linearly coupled, and we numerically solve for velocity, $\vec{u}$, pressure, p, electrical potential, ϕ, and ion concentrations, $c_\pm$.

The boundary conditions for the above governing Eqs. are illustrated in Fig.1b. Along the nanochannel wall, a combination of no-slip ($u_t = \vec{u}\cdot\vec{t} = 0$) and no-penetration ($u_n = \vec{u}\cdot\vec{n} = 0$) conditions are implemented. A constant flow velocity, v_f, was applied at the inlet and outlet of the reservoirs in this steady-state model. Solutions of different salt concentrations (c_H and c_L at left side and right side reservoir, respectively) flow in through the two reservoirs. The reservoir size is 50 nm × (50+h) nm for a given nanochannel of height of h. The surface charge density of the nanochannel, σ, was assumed constant and positive here. This boundary condition can be modeled as: $\partial\phi/\partial y = -\sigma/\epsilon_0\epsilon_r$, via the discontinuity of the electrical field in the direction normal to the surface due to a net surface charge [63]. The value of σ was varied as a control parameter. There was no external pressure difference applied to this nanofluidic setup. The boundary stress S_B ($= -p + 2\mu\partial u/\partial n$) was assumed to be zero along the reservoir boundaries as shown in Fig.1b.

III. NUMERICAL SIMULATIONS

The numerical simulations were implemented in 2D Cartesian coordinates, based on a finite element model using COMSOL Multiphysics 5.3. We verified our numerical simulations by comparing our results with existing analytical and numerical results of simplified cases related to DOF and EOF flows.

We first validated our numerical model with an analytical solution of electrokinetic flow of a dilute electrolyte under an external electrical field by Burgreen and Nakache [67]. In the theoretical analysis without any external flow or concentration difference, they formulated the generation of streaming potential in fine capillaries and analyzed the dependence of the resultant flow on the channel radius and Debye length. This 1D analytical simulation, based on surface potential, ζ, has been compared with our (modified) 2D numerical simulation, based on surface charge density, σ, using the Grahame relation: $\sigma = \epsilon_0\epsilon_r\zeta/\lambda_D$ [68]. Illustrated in Fig. 2, the transverse electric potential profile (non-dimensionalized by the surface potential, ϕ_0) of our (simplified) 2D simulation (with $v_f = 0$) agree well with the 1D analytical solutions of the electrokinetic flow by Burgreen and Nakache [67], with an average relative percentage error of ≈ 5%.

In addition, we benchmarked our simulation with an investigation of electrohydrodynamic transport by Pivonka et al. [69]. They reported transport of ionic solution across a negatively-charged slit opening subjected to an electrolyte concentration gradient, but without external electrical forcing. The nano-slit was connected to two steady reservoirs with no external flow (i.e., $v_f = 0$). With appropriate modifications in our simulation, by implementing h = 10 nm, l = 150 nm, $\sigma = -0.01$ C/m^2, c_L = 10 mM and c_H = 20 mM, we

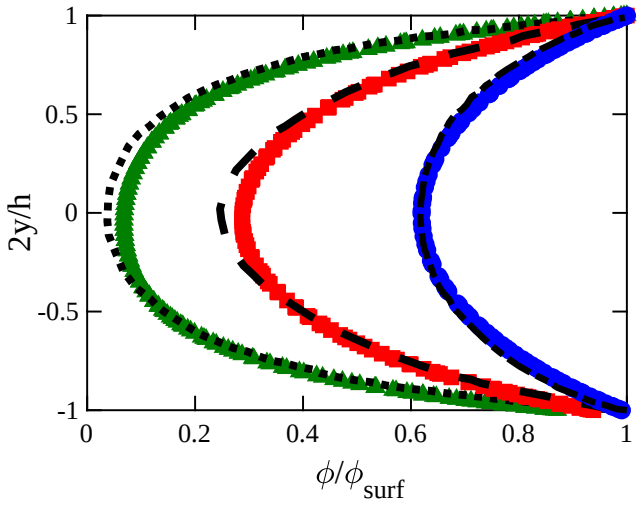

FIG. 2. Comparison of non-dimensional electric potential (by the surface potential) along the transverse direction (y-axis) of our two-dimensional (simplified) numerical simulation with one-dimensional analytical results of electrokinetic flow under an external electric field without external flow nor external concentration difference, reported by Burgreen and Nakache [67]. The numerical results are shown for different electrokinetic radii of $h/\lambda_D = 1$ (●), 2 (■) and 4 (▲), compared with the corresponding analytical results (shown by a dotted-dashed, dashed, and dotted line, respectively) by Burgreen and Nakache [67].

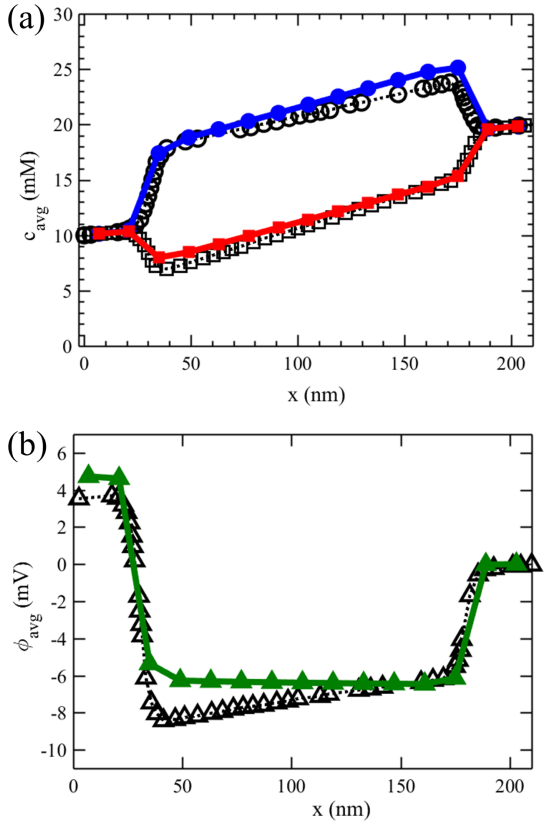

FIG. 3. (a) Average cationic (●) and anionic (■) concentrations, and (b) average electric potential (▲) obtained by our simplified numerical model of diffusioosmotic flow without external flow (i.e., the current model for steady reservoirs, but with $v_f = 0$). The corresponding comparisons are done based on the numerical results (○, □, and △) by Pivonka et al. [69]. Here, we investigated a 2D steady diffusioosmotic flow through a negatively charged slit (of height $h = 10$ nm, length $l = 150$ nm, $D = 2D_+$, and surface charge density $\sigma =$ -0.01 C/m^2). The nano-slit is connected to two reservoirs (of dimensions 30 nm × 30 nm) with electrolyte concentrations of $c_L = 10$ mM and $c_H = 20$ mM.

compared our results with the numerical investigations of Pivonka et al. [69]. Shown in Fig. 3 are the simulation results of the average cation and anion concentrations over the cross-section (in (a)) and average electric potential (in (b)) along the nanochannel. Although approximately 10% deviation of average electric potential is present inside of the nano-slit (shown in Fig. 3 (b)), the average cation and anion concentrations between the two numerical models agree well, with approximately 5% deviation (see Fig. 3 (a)). We further investigated this discrepancy for the average electric potential and compared the membrane potential (i.e., the potential difference across the nanochannel) between our results ($\Delta\phi \approx 4.8$ mV) with those reported by Westermann-Clark and Christoforou [70] ($\Delta\phi_2 = 5.7$ mV), which demonstrated a better agreement when compared to Pivonka et al. ($\Delta\phi \approx 3.2$ mV). The deviation between our simulation data and those by Pivonka et al. may be attributed to the lower mesh number (2336 elements) used in their study, whereas a greater number of mesh elements (> 20,000) in our case.

We also carried out mesh-independence tests, where convergent values of electrical potential difference and nanochannel resistance were obtained [20]. When the total number of (computational finite) elements is greater than 20,000, the reproducibility of the results is enhanced significantly (with the deviations within ≈ 4%). Therefore, the typical mesh number for all computations were greater than 20,000.

IV. RESULTS AND DISCUSSIONS

We numerically studied the influences of nanochannel dimensions (height h, length l), surface charge density (σ), and electrolyte concentrations (c_H, c_L) on 2D DOF driven by electrical interaction and chemical diffusion processes. For the 2D nano/micro-junction geometry, due to the nonlinear and coupled Eqs. (1) – (5), we carried out more than 100 simulations in total, by varying the ranges of the key parameters: $l = 40 - 200$ nm, $h = 15 - 150$ nm, $\sigma = 0.001 - 0.05$ C/m^2, $c_H = 0.01 - 1$ mM, with a fixed $c_L = 0.01$ mM. Here, the wall's surface charge, σ, studied has a similar range to that of anodic alumina nanopores [17], while a similar range but

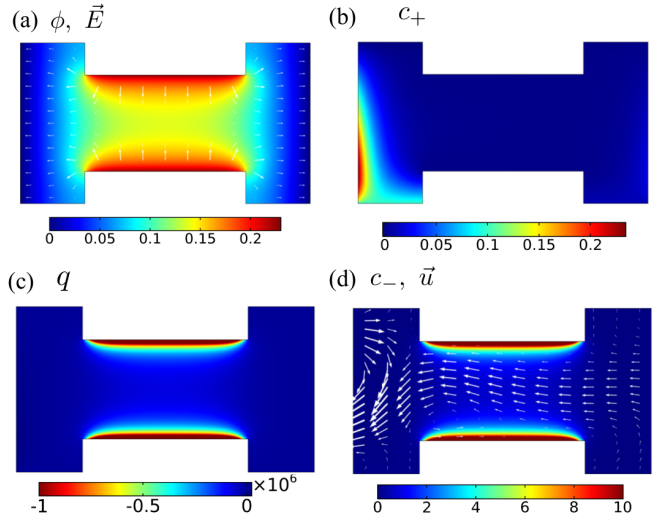

FIG. 4. Simulation results of (a) electric potential ϕ (Volts) and field $\vec{E}$ (V/m), in arrows, (b) cation concentration profile c_+ (mM), (c) net charge q (C), and (d) anionic concentration c_- (mM) with velocity field $\vec{u}$, in arrows, for the nanochannel parameters of $h = 60$ nm, $l = 100$ nm, $c_L = 0.01$ mM, $c_H = 0.15$ mM, $\sigma = 0.01$ C/m^2, and $v_f = 0.07$ mm/s.

negative charges are present for glass and silica interfaces [71].

A. Effect of nanochannel dimensions

Shown in Fig. 4 are the numerical results for a medium-sized charged-nanochannel of $h = 60$ nm, where the electric double layers adjacent to the wall do not overlap. Fig. 4a shows the distributions of electric potential, ϕ, as well as the electric field, $\vec{E}$ (in white arrows). The notable variation of electric potential in the transverse direction demonstrates the non-overlap of EDL. Without an external electric field, the imposed positive surface charge along the nanochannel leads to positive and maximal ϕ adjacent to the charged wall. The electric field $\vec{E}$ ($= -\vec{\nabla}\phi$) directs outward from high towards low electrical potential (i.e., outwards from the nanochannel towards the two reservoirs at the junction and outwards from the charged wall towards the center inside the nanochannel).

Fig. 4b shows that the distribution of cationic concentration, c_+, for the case of $h = 60$ nm. The figure illustrates a higher cationic concentration in the high electrolyte concentration reservoir (of c_H) due to Coulombic repulsion from the positive-charged nanochannel surface. As illustrated in Fig. 4c, negative charges accumulate close to the positively charged nanochannel, whereas a large fraction of neutral charges are present across the nanochannel. Fig. 4d reveals that anions accumulate right adjacent to the nanochannel wall because of positive surface charge, and the overall nanoflow field is directed from the reservoir of low towards high concentration. For a larger h, the electrical neutrality of nanochannel leads to a weaker electroosmotic effect, and flow is driven primarily by chemiosmosis. Under a concentration gradient between the two reservoirs, water molecules move from c_L to c_H towards equilibrium, thereby producing such flow direction.

Fig. 5 shows the numerical results for a narrow channel of height, $h = 10$ nm. Studying this nanochannel configuration with an overlapping Debye length is important for understanding the inherent mechanism of the charge selectivity and the resultant flow inside the nanochannel. The electric potential (ϕ) profile in the 2D geometry is shown in Fig. 5a, along with the electric field ($\vec{E}$) in arrows. Due to the overlapping of EDL in this case of $h = 10$ nm, ϕ is, hence, positive within the entire nanochannel, and the variation of ϕ along the width of the nanochannel is less significant when compared with that of $h = 60$ nm.

Fig. 5b reveals a low cation concentration in the nanochannel since the cations as co-ions are repelled away from the positively charged nanochannel. Therefore, in the high concentration reservoir, cations also accumulate in the left bottom corner. In contrast, as counter-ions, the anion concentration, c_-, increases significantly inside the nanochannel, resulting in a net negative charge within the nanochannel, as illustrated by Fig. 5c. Unlike the case of non-overlap of EDL ($h = 60$ nm), electrical neutrality is not seen in majority of the nanochannel of $h = 10$ nm. Therefore, there is a stronger electroosmosis dominating the flow for $h = 10$ nm, compared to that of $h = 60$ nm. The distribution of

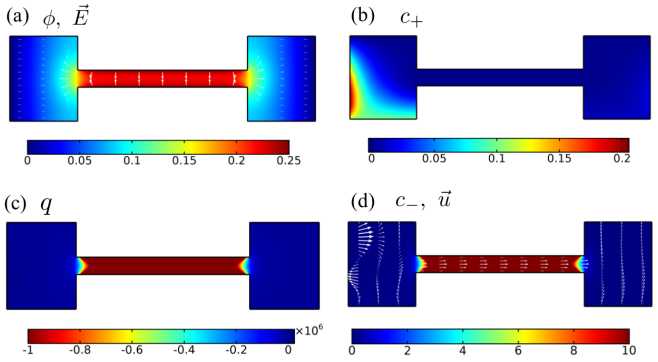

FIG. 5. Numerical results of the steady-state diffusioosmotic flow in nano/micro-junctions, showing (a) electric potential ϕ (Volts) with electric field $\vec{E}$ (V/m) in arrows, (b) cation concentration c_+ (mM), (c) net charge q ($= z_+c_+ + z_-c_-$) (in C), and (d) anionic concentration c_- (mM) with flow velocity $\vec{u}$ in arrows. The parameters used are $h = 10$ nm, $l = 100$ nm, $c_L = 0.01$ mM, $c_H = 0.15$ mM, $\sigma = 0.01$ C/m^2, and $v_f = 0.07$ mm/s.

anion concentration (c_-) and velocity profile are shown in Fig. 5d. Due to the ion-selective effect of the nanochannel with overlapping EDL, the cation concentration inside the nanochannel is negligible; hence, the net charge profile (Fig. 5c) and the anion distribution (Fig. 5d) looks identical. In this simulation case of $h = 10$ nm, the flow direction inside the nanochannel is from high concentration (c_H) reservoir to the low concentration (c_L) one, opposite to that for the $h = 60$ nm case shown in Fig. 4d. Based on our simulation result for the narrow, charged nanochannel of $h = 10$ nm, there is a net electrical field in the x-direction pointing towards left, with a dominant anion concentration, inside the nanochannel, resulting in an electrical body force, $F_e\hat{x} = q\vec{E}_x$, where q is negative, thereby pointing towards right. This electrical body force within the EDLs leads to a dominant electroosmotic flow, driving the flow towards right (in the direction from c_H to c_L) for $h \approx 10$ nm (see Fig. 5d), whereas the chemiosmosis effect is weak since negligible anion concentration difference inside of such charged, nanochannel was observed.

In brief, in the absence of external electrical forcing, the local electric field and ion-concentration distributions direct the overall flow in a narrow nanochannel with EDL overlap ($h = 10$ nm) from the reservoir of high concentration (c_H) to that of low concentration (c_L), as explained above. Interestingly, the direction of this bulk flow in a charged, narrow nanochannel with overlapping EDL is reversed, compared to that for a wide nanochannel without EDL overlapping. This reversal of flow direction by tuning nanochannel dimensions can have useful applications in nanofluidic devices for flow control.

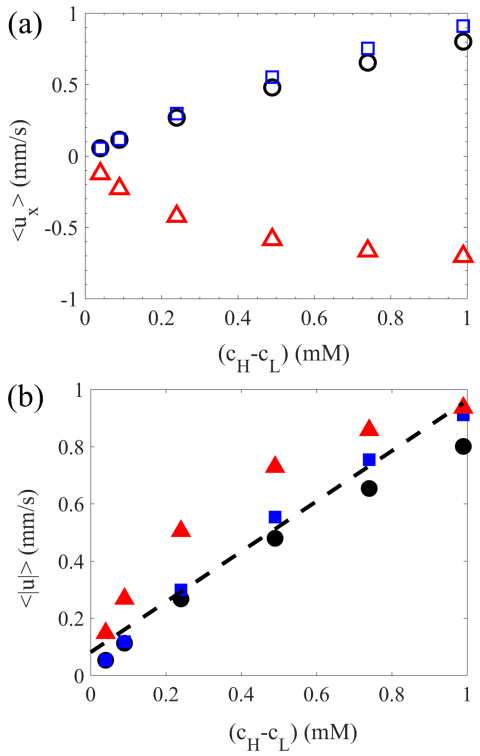

FIG. 6. Effect of concentration difference on the nanoflow velocity for $l = 100$ nm: (a) Average nanoflow velocity in x-direction, $\langle u_x \rangle$ and (b) Net average nanoflow velocity, $\langle |u| \rangle$. Different symbols represent different nanochannel height used: $h = 10$ nm (● and ○), $h = 30$ nm (■ and □), and $h = 60$ nm (▲ and △). The dashed line (- - -) shows the best linear fit, with a slope of 0.88.

B. Influence of electrolyte concentration difference

The effect of electrolyte concentration gradient on the flow velocity was also studied. Illustrated by Fig. 6, the numerical results show that the magnitude of average flow velocity $\langle |u| \rangle$ in the nanochannel is primarily governed by the concentration difference Δc ($= c_H - c_L$) between the two reservoirs. As shown in Fig. 6b, $\langle |u| \rangle$ increases linearly with Δc for $0 \lesssim \Delta c \leq 1$ mM simulated. We carried out a best least-square residual fitting (of $A_1 \Delta c + A_0$) and found the best linear coefficient $A_1 \approx 0.88$. The value of this linear fitting coefficient is consistent with that estimated using a characteristic diffusioosmotic flow speed, $|U| = \frac{2RT\lambda_D^2}{\mu}|\nabla c|$, predicted by Keh et al., for a constant ∇c along a flat charged surface with ions following the Poisson-Boltzmann distribution [33]. To perform an order of magnitude comparison, we estimated $\nabla c \simeq \Delta c/l$ by dimensional analysis and assumed constant c and λ_D for our simulation cases; thus, $|U| \simeq \frac{2RT\lambda_D^2}{\mu l}\Delta c$. We estimated λ_D based on an average anion concentration of 5.48 mM for our simulation case, that is $\lambda_D \approx 4$ nm. Hence, the theoretical linear coefficient was estimated to be 0.87, which is consistent with the linear-fit result of 0.88 found from our numerical data.

From our numerical results, surprisingly, the value of Δc (when $\Delta c > 0$) does not play an important role in determining the nanoflow direction. Nanoflow in both directions is observed for a wide range of Δc imposed (see Fig. 6a). The nanochannel size, on the other hand, influences the nanoflow direction significantly. As shown in Fig. 6a, narrower nanochannels (h = 10, 30 nm) tend to have an electroosmosis dominated flow due to the net (negative) charges in the nanochannel with an overlapping Debye length. For the narrow nano/microjunctions, electrical body force is strong and dominating in the region close to c_H with the electrical body force towards left (i.e., in the horizontal direction from c_L to c_H). As a result, for small $h(\approx 10$ nm) the electroosmotic effect dominants with a significant anion concentration (having a net negative charge) under a left-pointing E_x inside the charge nanochannel, leading to a strong electrical body force moving the nanoflow towards right (in the horizontal direction from the high (c_H) to low concentration (c_L) reservoir. Conversely, for a relatively large nanochannel (e.g. $h = 60$ nm), with a significant fraction

of neutral charges, the nanoflow is determined primarily by a diffusion process under Δc, causing the nanoflow (with water molecules) to move from c_L to c_H reservoir due to a dominant chemiosmosis.

C. Controlling nanoflow direction

Our simulation results examining the influence of σ, c_H, c_L, h, and l on a steady-state diffusioosmotic flow show three different modes of flow in the charged nanochannel. These distinct modes of nanoflow encompass different flow directions: (i) opposite, (ii) parallel to the direction of concentration gradient, and (iii) a mixture mode of these two directions. By analyzing and plotting different nanoflow regimes against different control parameters, we found that nanoflow direction is primarily controlled by merely a few key parameters for the parameter ranges explored. These major influences are (1) nanochannel height (h), (2) nanochannel length (l), and (3) surface charge density (σ). We noticed that the values of c_H (ranging from 0.001 – 1 mM) and Δc (with a fixed c_L of 0.01 mM) have an insignificant influence on the nanoflow direction.

Revealed in Fig. 7 is the influence of diffusioosmosis on nanoflow direction from more than 40 simulations at different h, L and σ, keeping other parameters constant (c_L = 0.01 mM, c_H = 1 mM, v_f = 0.07 mm/s). Since charge-selectivity of nano-confinements is dictated by the extent of overlap of EDL [8], it is also important to see its effect on DOF. We, thus, investigated the variation of diffusioosmotic velocity $\langle u_x \rangle$ with h/λ_D, where λ_D is the Debye length (estimated using the average concentration of anions inside nanochannel). However, as evident from in fig. 7e, in the case of our 2D geometry focusing on micro/nano-junction applications, the ratio h/λ_D does not seem to be the most vital parameter in determining the direction of diffusio-osmotic flow.

Through the phase diagram analyzing the effects of σ, h and l on direction of diffusioosmotic flow (Fig. 7a) and scaling analysis, we found a non-dimensional number, C, which can be used to collapse our data separating different nanoflow regimes and predict the direction of DOF through a nanochannel with the known values of l, h, and σ:

$$C = h/\sqrt{l\lambda_{GC}}, \tag{6}$$

where λ_{GC} is known as Gouy-Chapman length, a characteristic length based on the surface charge density (σ) of the nanochannel, and can be estimated as [72, 73]: $\lambda_{GC} = \frac{2\epsilon_0\epsilon_r RT}{\sigma F z}$. The Gouy-Chapman length, λ_{GC}, is related to Bjerrum length, λ_B, via $\lambda_{GC} = \frac{e}{2\pi\sigma\lambda_B}$, where λ_B ($=z^2e^2/4\pi\epsilon_0\epsilon_r k_B T$) is a characteristic distance at which the electrostatic interaction between two charged species in a solution is comparable to the thermal energy [5]. The dimensionless number, C, indicates the ratio of the nanochannel height, h, to a characteristic length scale, $\sqrt{l\lambda_{GC}}$, which can be associated with the influence of electrical interaction over a length-scale of $\approx \lambda_{GC}$ due to the nanochannel surface charge along the channel length, l.

Fig. 7f illustrates the variation of average diffusioosmotic velocity in x-direction, $\langle u_x \rangle$, with the characteristic parameter C given in Eq. (6). Below a critical value of $C \simeq 1.75$, the nanoflow is directed from the reservoir of high concentration (c_H) to that of low concentration (c_L), as for the case of narrow h, e.g., 10 nm shown in Fig. 5d. Above the value of $C \simeq 2.2$, the bulk nanoflow is in the opposite direction, from the low (c_L) to the high (c_H) concentration reservoir, similar to the case of large h = 60 nm revealed by the flow field in Fig. 4d. In between these two critical values, circulation and mixing are present inside the nanochannel. These critical values of C were calculated based on the range of surface charge (σ) explored, between 0.001 and 0.05 C/m^2. These numerical values of critical C are very likely specific to the complex 2D nano/micro-junction geometry considered.

In addition, our simulation results in Fig. 7f show that most of $C \approx 2$ data are for the reversal cases (upper red symbols in Fig. 7f) for different h, l, and σ, whereas the three data points for $C \approx 2$ (of lower blue symbols in Fig. 7f) are all from small σ (0.001 C/m2), relatively large h (= 110−140 nm), and a comparable l (= 100−140 nm), although a larger h ($\approx$ 150 nm) can also generate the normal flow directions showing a positive $< u_x >$. Therefore, from the simulation results we can conclude that most cases show flow reversal when $C \lesssim 2$, however with a few exceptions for the parameters with a small σ, a relative large h (= 110−140 nm) and with a comparable l, whereby the surface charge effect is weak.

In comparison, previous theoretical study of diffusioosmosis flow under a homogeneous concentration gradient along a charged flat plate shows that Zeta potential [41] or channel aspect ratio [34] plays an important role in the direction of the nanoflow. For our complex flow geometry of nano/micro-junction, we found that C is a better parameter delineating different flow regimes, as demonstrated by the comparison between Fig. 7e and 7f. The non-dimensional number, C, can be physically interpreted through the interaction or comparison between electroosmotic and chemiosmotic effect, which is briefly explained below and in details in Supplementary Information (SI).

On the one hand, electro-osmotic velocity, u_{EO}, is caused by electro-migration of ions due to an external electric field or an induced one (due to interaction between surface charge and ions via a concentration gradient). Under the effect of a tangential electric field, E_x, it can be shown that u_{EO} for a charged nano-confinement of constant zeta potential (ζ) along its surface is represented as [28, 74, 75]:

$$u_{EO} = -\frac{\epsilon\zeta E_x}{\mu}, \tag{7}$$

where ϵ ($= \epsilon_0\epsilon_r$) is the permittivity of the medium, and

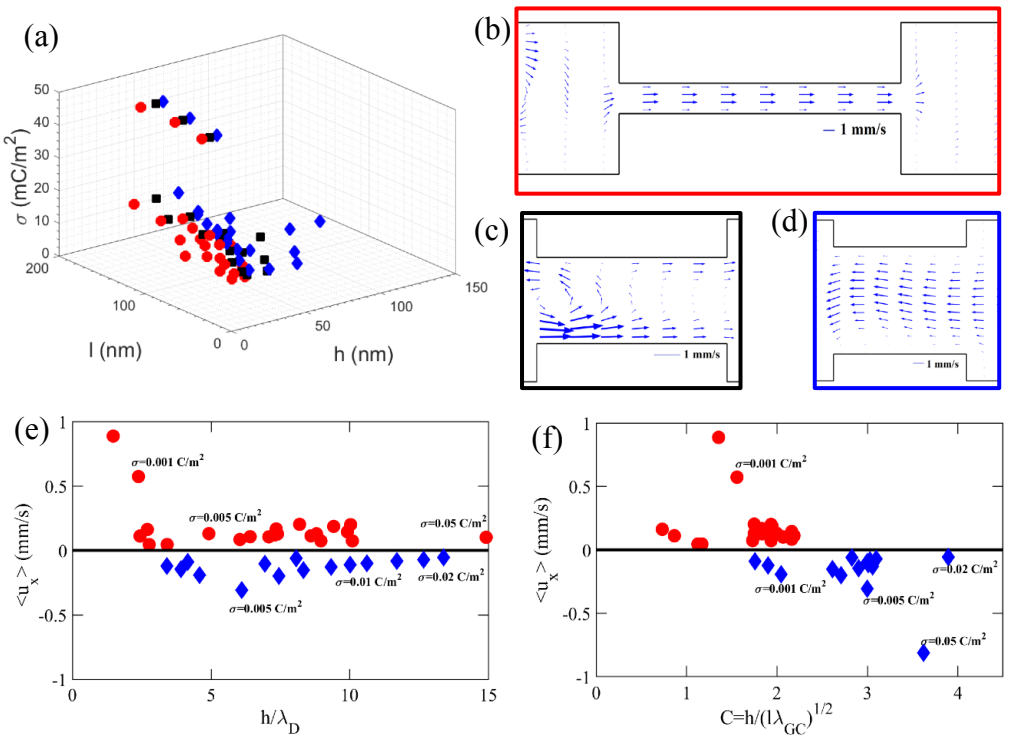

FIG. 7. (a) Phase diagram of diffusioosmotic nanoflow revealing different flow directions for different nanochannel parameters of h, l, and σ. Flow regime (I), denoted by ●, represents the flow from high to low concentration reservoir; Regime (III) ♦ represents the flow from low to high concentration reservoir; Regime (II), denoted by ■, represents the mixed flow of both directions. Representative flow profiles observed inside the nanochannels are shown for (b) Regime (I), (c) Regime II, and (d) Region III. Variation of (e) h/λ_D, and (f) a critical non-dimensional parameter, C ($= h/\sqrt{l\lambda_{GC}}$), with average velocity in x-direction inside nanochannel, $< u_x >$. In this analysis, 5 different values of σ in the range of 0.001 – 0.05 C/m^2 have been used, as denoted in (e) and (f). The ranges of nanochannel height and length explored are $h = 15 - 150$ nm and $l = 40 - 200$ nm.

μ is the fluid viscosity coefficient. As $E_x = -\partial\phi/\partial x\ \hat{x}$, while the electrical potential, ϕ, depends on spatial net charges (q) and, hence, ion concentrations ($c_\pm$), which nonlinearly depends on the local diffusive, electromigration, and convective ion fluxes, i.e., by solving the coupled Eq. (1)-(5). Therefore, finding a simple analytical form of E_x for this nonlinear system is challenging. Based on our numerical results by analyzing electrical field E_x inside the charged nanochannel, we found $|E_x| \approx |E_y|$ in terms of magnitude.

To estimate the magnitude of the electric field $|E_x|$, assumed to be $\approx |E_y|$, which can be calculated using the boundary condition of constant surface charge density [63], via $\vec{\nabla}\phi \cdot \vec{n} = -\sigma/\epsilon$, so E_y scales with σ/ϵ. Eq. (A1) then can be estimated with

$$u_{EO} \simeq -\frac{\zeta\sigma}{\mu}. \tag{8}$$

On the other hand, when a nanochannel is subjected to a solution concentration difference, Δc, along its length, a chemical potential gradient develops and initiates fluid flow from one reservoir to another. This flow, known as chemiosmotic velocity, u_{CO}, can be derived and expressed as [31, 74]:

$$u_{CO} = -\frac{k_B T}{\mu}\frac{\ln(1-\gamma^2)}{2\pi\lambda_B}\frac{\Delta c}{l c_0}, \tag{9}$$

where $\gamma = \tanh\frac{ez\phi_s}{4k_BT}$, ϕ_s is the surface potential, z is the valence of ions, e is the electronic charge, k_B is the Boltzmann constant, and T is the temperature. c_0 is the reference solution concentration, λ_B is the Bjerrum length and related to the Gouy-Chapman length, λ_{GC}, as defined above. For the dilute electrolyte concentrations explored, after considerable simplification (for example, using the linearized Boltzmann distribution of ions [62]) described in detail in SI, we obtained the ratio of chemiosmotic velocity (Eq. (A4)) and electro-osmotic velocity (Eq. (A3)) to compare the effect of chemiosmosis *vs.* electroosmosis:

$$\left|\frac{u_{CO}}{u_{EO}}\right| \approx \frac{1}{8}\left(\frac{ez\phi_s}{k_BT}\right)^2\frac{\lambda_{GC}}{l}\exp\left(-\frac{y}{\lambda_D}\right). \tag{10}$$

To estimate the surface potential (ϕ_s), its gradient along the charged surface can be estimated using the

surface charge BC, $\vec{\nabla}\phi \cdot \vec{n} = -\sigma/\epsilon \sim \partial\phi/\partial y \sim \phi_s/h$. Surface potential can then be estimated as $\phi_s \simeq -\sigma h/\epsilon$. We substitute this expression for ϕ_s into Eq. (A11) and obtain:

$$\left|\frac{u_{CO}}{u_{EO}}\right| \approx \frac{1}{2}\frac{h^2}{\lambda_{GC} l} \exp\left(-\frac{y}{\lambda_D}\right) \approx \frac{1}{2} C^2 \exp\left(-y/\lambda_D\right), \tag{11}$$

where C $(= h/\sqrt{l\lambda_{GC}})$ is the non-dimensional number characterizing the direction of nanofluidic transport inside the nanochannel. For $y \ll \lambda_D$, $\exp(-y/\lambda_D) \approx 1$, and thus, $|\frac{u_{CO}}{u_{EO}}| \approx \frac{C^2}{2}$. This allows us to express the critical C, $C^* = \sqrt{2}$ when $u_{CO} \approx u_{EO}$. In other words, the characteristic parameter, C, can characterize the dominance of either chemiosmotic ($C > C^*$) or electroosmotic ($C < C^*$) flow. From our numerical data shown in Fig. 7f, we observed a critical $C^* \approx 1.98 \pm 0.22$, which is consistent with this simplified theoretical prediction of $C^* = \sqrt{2}$ (≈ 1.41).

Based on charge conservation described by Eq. (2), diffusioosmotic flow is governed by diffusion, electromigration, and advection. When the nanochannel is narrow and long with sufficiently large Gouy-Chapman length, i.e., equivalent to a smaller value of C, the electromigration term dominates, and due to charge selectivity of the nanochannel, anionic flow is dominant in the nanochannel and supplied by the solution flowing from the high to the low concentration reservoir (fig. 7b). Conversely, for wider and shorter channels of a relatively small Gouy-Chapman length (i.e., a large C), electroosmotic effect diminishes due to almost neutral electric field induced in the bulk. Consequently, the chemiosmotic effect dominates, with water molecules moving from low to high ion concentration area (fig. 7d). However, very close to the channel, the electromigration of ions is still dominant within the EDL. In intermediate scenarios, both chemiosmotic and electroosmotic flows exist and are comparable, and hence a combination of these effects causes circulation and mixing in the nanoflow (fig. 7c).

For future research directions, the present numerical framework, concerning diffusioosmosis in a charged nanochannel connecting to two side reservoirs of different electrolyte concentrations, is a common theme in water purification and sustainable energy generation using reverse electrodialysis (RED) and can be extended to investigate electric transport of current and ionic fluxes [10], nanofluidic transport using concentrated electrolyte solutions, and associated diffusiophoresis effect on colloidal particle motions [76]. In addition, with nonlinear, nonlocal, and coupled governing equations, our numerical framework can be extended to examine the influences of external pressure gradient, applied electric voltage, nanochannel slip length [5, 10, 77], high-salinity electrolytes [10], and diffusivity difference between cations and anions [33] on various intriguing electrokinetic phenomena, affecting desalination, membrane filtration, and RED processes and efficiencies using charged nano-channels or pores.

V. CONCLUSIONS

We investigated the effects of the nanochannel dimensions and surface charge on diffusioosmotic flow in a charged nanochannel connecting two reservoirs of different electrolyte concentrations, which is a common flow geometry for reverse electrodialysis and micro/nanojunctions. In the parameter ranges explored, we empirically quantified a critical non-dimensional number $C = h/\sqrt{\lambda_{GC} l}$ that can essentially predict the direction of the nanoflow, thereby affecting the convective electrical flux in the nanochannel. This dimensionless number, C, was found by comparing the relative strength of electrosmotic and chemioosmotic components of DOF in our 2D setup. While electrosmosis is governed by the electric field in a system, chemioosmosis is dictated by the corresponding ionic concentration gradient in the nanoflow.

Through rigorous comparison, and scaling analysis, the ratio of electric and chemioosmotic flow was found to be dependent on three key nanochannel parameters, namely, the nanochannel height (h), length (l) and surface charge density (σ). Fundamentally, the dimensionless constant C describes a ratio of nanochannel height to surface charge effect, where $\sqrt{\lambda_{GC} l}$ may indicate a length-scale, characterizing the effect of surface charge (σ) along the nanochannel length (l). A high value of C ($\gtrsim 1.98$) indicates an insignificant electroosmosis, and due to chemiosmosis water flows from low to high concentration reservoir for a positively charged nanochannel. In contrast, for a lower value of C ($\lesssim 1.98$) electroosmosis directs nano-DOF from the high to low concentration reservoir (against the concentration gradient) due to local electrical body force in the nanochannel. The nanoflow speed is, however, independent of this non-dimensional number, C, but linearly depends on the concentration difference.

Our simulation results, along with the theoretical analysis, reveal the key quantitative parameter, C, for controlling nanoflow by tuning the nanochannel parameters of length, height, and surface charge. Our results further imply that typical nanotube dimensions (of h $\approx$ 1 nm and l = 1 − 10 nm), with a maximum σ = 0.05 C/m^2 and c_H ranging between 0.01 and 1 mM, give rise to a small C < O(0.1) and a reversal flow with dilute electrolytes. Experimentally, local nanoflow velocity is challenging to measure directly since well-established micro-particle velocemetry technique is not applicable for nanoscale flows and fluorescent dyes are often charged, while the global measurements of flow rates in nanochannels are more feasible [54, 55, 78, 79]. In terms of applications, the quantification of the nanoflow direction is important for building nanofluidic devices enabling flow control, currently attracting attention towards nanofluidic desalination, water purification, and reverse electrodialysis. The dimensionless parameter C presented and its critical value can help predict the diffusioosmotic flow directions, conveniently using three crucial nanochannel parameters: height, length, and surface charge.

CONFLICTS OF INTEREST

There are no conflicts to declare.

DATA AVAILABILITY

The data that supports the findings of this study are available from the corresponding author upon reasonable request.

ACKNOWLEDGEMENTS

S. C. acknowledges the support of graduate student scholarship from Alberta Innovate Technology Futures (AITF). P. A. T. acknowledges Natural Sciences and Engineering Research Council (NSERC) of Canada for the Discovery and Accelerator grants as well as Canada Research Chair Program in Fluids and Interfaces.

Appendices

A. ADDITIONAL VALIDATIONS OF THE NUMERICAL SIMULATION

We further validated our COMSOL simulation by a comparison with the results reported by Kang et al. [17]. As shown in Fig. 8, we found a good agreement between Kang et al. findings [17] and our results for a simplified model without external flow.

B. SIMULATION RESULTS OF ANIONIC FLUXES

In Appendix B, we provide the anionic fluxes, J_- based on Eq. (3) consisting of diffusive, electromigration and convective ionic species, for the same numerical cases as Fig. 4 and 5. In these cases, illustrated by Fig. 9, higher anionic flux occurs near the regions of higher local concentration gradient. The anionic flux hence is maximum near the electric double layer.

C. FORMULATION OF NON-DIMENSIONAL NUMBER C

In Appendix C, we discuss the analytical derivation of the characteristic non-dimensional number (C), introduced in the main paper using scaling analysis and classical theories of electrokinetic flow. Diffusioosmotic flow through a nanochannel is affected by two phenomena, namely electroosmosis and chemiosmosis. The critical parameter, C^*, is derived as the ratio of chemiosmotic to electroosmotic flow velocity and a primary parameter controlling the nanoflow direction in a charged nanoconfinement. The physical interpretation of the non-dimensional number is obtained through the simplified expressions of the classical chemiosmotic and electroosmotic velocities, described below.

B1. Electro-osmotic velocity

On one hand, electro-osmotic velocity, u_{EO}, is caused by electro-migration of ions due to an external electric field or an induced one due to interaction between surface charge and bulk ions. Under a tangential electric field, E_x, without a chemiosmotic effect, it can be shown that u_{EO} for a charged nano-confinement of constant zeta potential, ζ, along its surface, can be represented as [28, 75]:

$$u_{EO} = -\frac{\epsilon \zeta E_x}{\mu}, \tag{A1}$$

where ϵ ($= \epsilon_0 \epsilon_r$) is the permittivity of the medium, and μ is the fluid viscosity coefficient. Electric field ($\vec{E}$) is a function of the electric potential, ϕ ($\vec{E} = -\vec{\nabla}\phi$); $E_x = -\partial\phi/\partial x\ \hat{x}$. Due to the complex nonlinearity of the diffusioosmotic problem for our nano/micro-junction geometry, a straight-forward analytical formulation of E_x, to the best knowledge of ours, is unavailable. From our numerical results, we observed that $|E_x| \approx |E_y|$ for the parameter ranges explored. We thus used this approximation to estimate $|E_x|$.

Along the charged nanochannel wall, $\vec{\nabla}\phi \cdot \vec{n} = \partial\phi/\partial y$, E_y close to the wall can be approximated using the boundary condition of constant surface charge density, σ: $\vec{\nabla}\phi \cdot \vec{n} = -\sigma/\epsilon$ [63], via

$$E_y = -\partial\phi/\partial y \approx \sigma/\epsilon. \tag{A2}$$

Using the relation (A2), we can estimate $E_x \approx E_y \approx \sigma/\epsilon$. Hence, Eq. (A1) can be approximated as:

$$u_{EO} \approx -\frac{\zeta\sigma}{\mu}. \tag{A3}$$

B2. Chemiosmotic velocity

On the other hand, when a nanochannel is subjected to a concentration difference of electrolytes, Δc, along its length, a chemical potential difference develops and initiates fluid flow to balance the chemical potential gradient. This flow is represented by the chemiosmotic velocity, u_{CO}, and can be expressed as [74]:

$$u_{CO} = -\frac{k_B T}{\mu} \frac{\ln(1-\gamma^2)}{2\pi\lambda_B} \frac{\Delta c}{l c_0}, \tag{A4}$$

where $\gamma = \tanh(ez\phi_s/4k_BT)$, ϕ_s is the surface potential, z is the valence of ions (while $z = 1$ in our case), e is

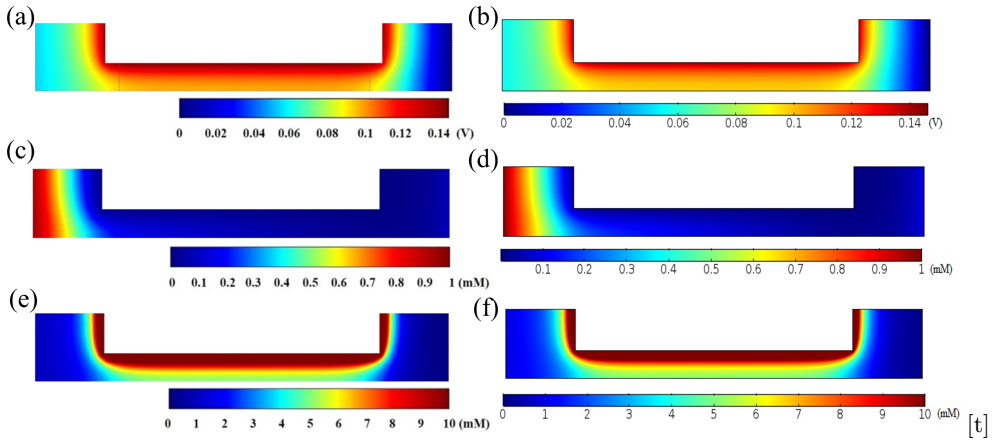

[t]

FIG. 8. Validation of the present numerical model based on the results by Kang et al. [17] $h = 10$ nm, $l = 100$ nm, $c_L = 0.1$ mM, $c_R = c_H/c_L = 10$, $\sigma = 0.01$ C/m^2, and $I_c = 0$. (a) Electrical potential profile, (c) cation concentration, and (e) anion concentration reported by Kang et al. The corresponding results by our simulation are shown in (b), (d), and (f), respectively.

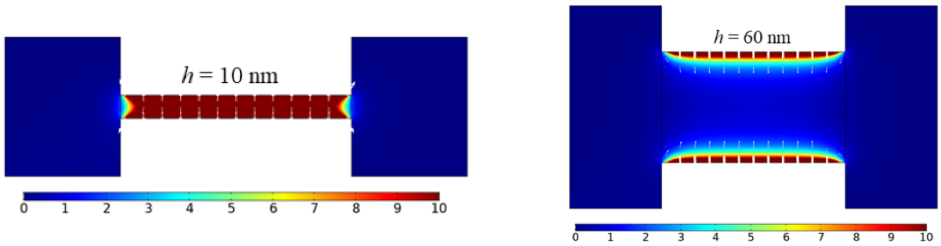

FIG. 9. The distribution of anionic concentration c_- and anionic flux field J_- (in arrows) for (a) $h = 10$ and (b) $h = 60$ nm. The other constant parameters are $l = 100$ nm, $c_L = 0.01$ mM, c_H =0.15 mM, $\sigma = 0.01$ C/m^2, and $v_f = 0.07$ mm/s.

the electronic charge, k_B is the Boltzmann constant, T is the temperature, and c_0 is the reference solution concentration. Here, λ_B is the Bjerrum length, mathematically described by $\lambda_B = z^2e^2/(4\pi\epsilon k_BT)$ [5], and related to the Gouy-Chapman length, λ_{GC} [5, 74]:

$$\lambda_{GC}\left(=\frac{2\epsilon RT}{\sigma Fz}=\frac{2\epsilon k_BT}{\sigma ez}\right)=\frac{ez}{2\pi\sigma\lambda_B}. \tag{A5}$$

Under the assumption that $\gamma^2 \ll 1$, we can approximate $\ln(1-\gamma^2) \approx -\gamma^2$ [26]. Further considering ϕ_s to be small such that $ez\phi_s/4k_BT \ll 1$, we get $\gamma = \tanh(ez\phi_s/4k_BT) \approx ez\phi_s/4k_BT$. Using Eq. (A5) and the above approximations, Eq. (A4) is simplified to:

$$u_{CO} \simeq \frac{k_BT\gamma^2}{\mu}\frac{\lambda_{GC}\sigma}{ez}\frac{\Delta c}{lc_0} \simeq \frac{ez\phi_s^2\lambda_{GC}\sigma}{16k_BT\mu}\frac{\Delta c}{lc_0}. \tag{A6}$$

With the consideration of Boltzmann distribution of ions [62] and subsequent linearization of the ion distribution, the concentration of cation (c_+) and anion (c_-) can be represented as [74]:

$$c_\pm \simeq c_0\left(1 \mp \frac{ez\phi_s}{k_BT}\exp\left(-\frac{y}{\lambda_D}\right)\right), \tag{A7}$$

where y is the direction perpendicular to the nanochannel surface.

Using the above linearized distribution of ion concentration, we can approximate the concentration difference, Δc ($\approx c_- - c_+$), as follows:

$$\Delta c \approx 2c_0\left(\frac{ez\phi_s}{k_BT}\exp\left(-\frac{y}{\lambda_D}\right)\right). \tag{A8}$$

Eq. (A6) can be simplified using the above relation:

$$u_{CO} \simeq \frac{1}{8}\left(\frac{ez\phi_s}{k_BT}\right)^2\frac{\lambda_{GC}\sigma}{l\mu}\exp\left(-\frac{y}{\lambda_D}\right)\phi_s. \tag{A9}$$

We calculate the ratio of the chemiosmotic (Eq. (A9)) to electroosmotic velocity (Eq. (A3)) to gauge the dominant effect of u_{EO} or u_{CO}:

$$\frac{u_{CO}}{u_{EO}} \approx \frac{1}{8}\left(\frac{ez\phi_s}{k_BT}\right)^2\frac{\lambda_{GC}\sigma}{l\mu}\exp\left(-\frac{y}{\lambda_D}\right)\phi_s\cdot\left(-\frac{\mu}{\zeta\sigma}\right). \tag{A10}$$

Here, the negative sign in the above ratio denotes that the chemiosmotic (u_{CO}) and diffusioosmotic (u_{EO}) flow are directed in opposite directions, and the final flow direction inside the nanochannel could be decided by the dominant effect.

Assuming surface potential, ϕ_s, to be approximately equal to the nanochannel zeta potential, ζ [68], we obtain a simplified expression of Eq. (A10):

$$\left|\frac{u_{CO}}{u_{EO}}\right| \approx \frac{1}{8}\left(\frac{ez\phi_s}{k_BT}\right)^2 \frac{\lambda_{GC}}{l}\exp\left(-\frac{y}{\lambda_D}\right). \tag{A11}$$

Potential gradient along the charged surface can be estimated as $\vec{\nabla}\phi\cdot\vec{n} = d\phi/dy \simeq \phi_s/h$. From this relation and Eq. (A2), surface potential can be approximated as $\phi_s \simeq -\frac{\sigma h}{\epsilon}$. We substitute this expression for ϕ_s into Eq. (A11) and use Eq. (A5) to obtain:

$$\begin{aligned}\left|\frac{u_{CO}}{u_{EO}}\right| &\approx \frac{1}{2}\frac{h^2}{(2\epsilon k_BT/ez\sigma)^2}\frac{\lambda_{GC}}{l}\exp\left(-\frac{y}{\lambda_D}\right) \qquad \text{(A12)}\\ &\approx \frac{1}{2}\frac{h^2}{\lambda_{GC}l}\exp\left(-\frac{y}{\lambda_D}\right)\\ &\approx \frac{1}{2}C^2\exp\left(-\frac{y}{\lambda_D}\right),\end{aligned}$$

where C $(= h/\sqrt{l\lambda_{GC}})$ is found to be a characteristic non-dimensional number that delineates nanofluidic DOF flow direction inside the nanochannel. For $y < \lambda_D$, $\exp(-y/\lambda_D) \approx 1-(y/\lambda_D)+O((y/\lambda_D)^2)$. For a simplified estimation, we consider $\exp(-y/\lambda_D) \simeq 1$, ignoring the remaining terms, and consequently $u_{CO}/u_{EO} \approx C^2/2$. This allows us to express the critical C, C^* to be equal to $\sqrt{2}$ when $u_{CO} \approx u_{EO}$. In other words, the non-dimensional parameter, C, can characterize the dominance of either chemiosmotic (when $C > C^*$) or electro-osmotic (for $C < C^*$) flow. Based on our numerical analysis and data, we found a critical $C^* \approx 1.98 \pm 0.22$, which is consistent with the analytical prediction of $C^* = \sqrt{2}$ (≈ 1.41).

[1] B. D. Gates, Q. Xu, M. Stewart, D. Ryan, C. G. Willson, and G. M. Whitesides, New approaches to nanofabrication: Molding, printing, and other techniques, Chem. Rev. **105**, 1171 (2005).

[2] A. Egatz-gomez, C. Wang, F. Klacsmann, Z. Pan, S. Marczak, Y. Wang, G. Sun, S. Senapati, and H.-C. Chang, Future microfluidic and nanofluidic modular platforms for nucleic acid liquid biopsy in precision medicine, Biomicrofluidics **10**, 032902 (2016).

[3] Y. Yan, Y. Wang, S. Senapati, J. Schiffbauer, G. Yossifon, and H. C. Chang, Robust ion current oscillations under a steady electric field: An ion channel analog, Phys. Rev. E **94**, 1 (2016).

[4] J. C. T. Eijkel and A. V. D. Berg, Nanofluidics : what is it and what can we expect from it ?, Microfluid. Nanofluidics , 249 (2005).

[5] L. Bocquet and E. Charlaix, Nanofluidics, from bulk to interfaces, Chem. Soc. Rev. **39**, 1073 (2010).

[6] L. Bocquet and P. Tabeling, Physics and technological aspects of nanofluidics, Lab Chip **14**, 3143 (2014).

[7] B. V. Derjaguin, S. S. Dukhin, and M. M. Koptelova, Capillary osmosis through porous partitions and properties of boundary layers of solutions, J. Colloid Interface Sci. **38**, 584 (1972).

[8] Z. Slouka, S. Senapati, and H.-C. Chang, Microfluidic Systems with Ion-Selective Membranes, Annu. Rev. Anal. Chem. **7**, 317 (2014).

[9] S. Samin and R. Van Roij, Solvo-osmotic flow in electrolytic mixtures, J. Fluid Mech. **819**, R11 (2017), 1703.06643.

[10] B. L. Werkhoven and R. Van Roij, Coupled water, charge and salt transport in heterogeneous nano-fluidic systems, Soft Matter **16**, 1527 (2020).

[11] S. J. Kim, S. H. Ko, K. H. Kang, and J. Han, Direct seawater desalination by ion concentration polarization, Nat. Nanotechnol. **5**, 297 (2010).

[12] D. Deng, E. V. Dydek, J.-h. Han, S. Schlumpberger, B. Zaltzman, and M. Z. Bazant, Overlimiting Current and Shock Electrodialysis in Porous Media, Langmuir , 1 (2013).

[13] S. Schlumpberger, N. B. Lu, M. Suss, and M. Z. Bazant, Scalable and Continuous Water Deionization by Shock Electrodialysis, Environ. Sci. Technol. Lett. , 367 (2015).

[14] S. Park, Y. Jung, S. Y. Son, I. Cho, Y. Cho, H. Lee, H.-y. Kim, and S. J. Kim, Capillarity ion concentration polarization as spontaneous desalting mechanism, Nat. Commun. **7**, 1 (2016).

[15] O. V. Hulko, B. J. Robinsin, and R. N. Kleiman, Fabrication of nanoscale single crystal InP membranes, Appl. Phys. Lett. **91**, 053119 (2007).

[16] F. Gertz, R. Azimov, and A. Khitun, Biological cell positioning and spatially selective destruction via magnetic nanoparticles, Appl. Phys. Lett. **101**, 013701 (2012).

[17] B. D. Kang, H. J. Kim, M. G. Lee, and D.-K. Kim, Numerical study on energy harvesting from concentration gradient by reverse electrodialysis in anodic alumina nanopores, Energy **86**, 525 (2015).

[18] M. Marino, L. Misuri, A. Carati, and D. Brogioli, Boosting the voltage of a salinity-gradient-power electrochemical cell by means of complex-forming solutions, Appl. Phys. Lett. **105**, 033901 (2014).

[19] S. H. Kwak, S.-R. Kwon, S. Baek, S.-M. Lim, Y.-C. Joo, and T. D. Chung, Densely charged polyelectrolyte-stuffed nanochannel arrays for power generation from salinity

gradient, Sci. Rep. **6**, 26416 (2016).
[20] S. Chanda and P. A. Tsai, Numerical simulation of renewable power generation using reverse electrodialysis, Energy **176**, 531 (2019).
[21] J. Moreno, S. Grasman, R. van Engelen, and K. Nijmeijer, Upscaling reverse electrodialysis, Environ. Sci. and Tech. **52**, 10856 (2018).
[22] H.-R. Jiang, N. Yoshinaga, and M. Sano, Active motion of a janus particle by self-thermophoresis in a defocused laser beam, Phys. Rev. Lett. **105**, 268302 (2010).
[23] M. Taghipoor, A. Bertsch, and P. Renaud, Thermal control of ionic transport and fluid flow in nanofluidic channels, Nanoscale **7**, 18799 (2015).
[24] P. B. Umbanhowar, V. Prasad, and D. A. Weitz, Monodisperse emulsion generation via drop break off in a coflowing stream, Langmuir **16**, 347 (2000).
[25] C. Bakli and S. Chakraborty, Capillary filling dynamics of water in nanopores, Appl. Phys. Lett. **101**, 153112 (2012).
[26] D. C. Prieve, Migration of a colloidal particle in a gradient of electrolyte concentration, Adv. Colloid Interface Sci. **16**, 321 (1982).
[27] H.-C. Chang, G. Yossifon, and E. A. Demekhin, Nanoscale Electrokinetics and Microvortices: How Microhydrodynamics Affects Nanofluidic Ion Flux, Annu. Rev. Fluid Mech. **44**, 421 (2012).
[28] R. Hunter, *Zeta Potential in Colloid Science: Principles and Applications* (Academic Press, 1981).
[29] H. J. Keh and L. Y. Hsu, Diffusioosmotic flow of electrolyte solutions in fibrous porous media at arbitrary zeta potential and double-layer thickness, Microfluid. Nanofluidics **7**, 773 (2009).
[30] S. S. Dukhin, Non-Equilibrium Electric Surface Phenomena, Adv. Colloid an.d Interface Sci. **44**, 1 (1993).
[31] D. C. Prieve, J. L. Anderson, J. P. Ebel, and M. E. Lowell, Motion of a particle generated by chemical gradients. Part 2. Electrolytes, J. Fluid Mech. **148**, 247 (1984).
[32] H. J. Keh and Y. K. Wei, Osmosis through a fibrous medium caused by transverse electrolyte concentration gradients, Langmuir **18**, 10475 (2002).
[33] H. J. Keh and H. C. Ma, Diffusioosmosis of electrolyte solutions along a charged plane wall, Langmuir **21**, 5461 (2005).
[34] V. Hoshyargar, S. Nezameddin Ashrafizadeh, and A. Sadeghi, Diffusioosmotic flow in rectangular microchannels, Electrophoresis **37**, 809 (2016).
[35] J. H. Wu and H. J. Keh, Diffusioosmosis and electroosmosis in a capillary slit with surface charge layers, Colloids Surfaces A Physicochem. Eng. Asp. **212**, 27 (2003).
[36] V. Hoshyargar, A. Sadeghi, and S. N. Ashrafizadeh, Bounded amplification of diffusioosmosis utilizing hydrophobicity, RSC Adv. **6**, 49517 (2016).
[37] V. Hoshyargar, S. N. Ashrafizadeh, and A. Sadeghi, Mass transport characteristics of diffusioosmosis: Potential applications for liquid phase transportation and separation, Phys. Fluids **29**, 012001 (2017).
[38] S. Marbach and L. Bocquet, Osmosis, from molecular insights to large-scale applications, Chem. Soc. Rev. **48**, 3102 (2019), 1902.06219.
[39] H. J. Keh and J. H. Wu, Electrokinetic flow in fine capillaries caused by gradients of electrolyte concentration, Langmuir **17**, 4216 (2001).
[40] H. B. Ma, C. Wilson, B. Borgmeyer, K. Park, Q. Yu, S. U. S. Choi, and M. Tirumala, Effect of nanofluid on the heat transport capability in an oscillating heat pipe, Appl. Phys. Lett. **88**, 143116 (2006).
[41] H. J. Keh and L. Y. Hsu, Diffusioosmosis of electrolyte solutions in fibrous porous media, Microfluid. Nanofluidics **5**, 347 (2008).
[42] D. M. Huang, C. Cottin-Bizonne, C. Ybert, and L. Bocquet, Ion-Specific Anomalous Electrokinetic Effects in Hydrophobic Nanochannels, Phys. Rev. E **98**, 177801 (2007).
[43] D. M. Huang, C. Cottin-Bizonne, C. Ybert, and L. Bocquet, Massive Amplification of Surface-Induced Transport at Superhydrophobic Surfaces, Phys. Rev. Lett. **101**, 064503 (2008).
[44] I. Cho, W. Kim, J. Kim, H.-y. Kim, H. Lee, and S. J. Kim, Non-Negligible Diffusio-Osmosis Inside an Ion Concentration Polarization Layer, Phys. Rev. Lett. **254501**, 1 (2016).
[45] H. Jeon, H. Lee, K. H. Kang, and G. Lim, Ion concentration polarization-based continuous separation device using electrical repulsion in the depletion region, Sci. Rep. **3**, 3483 (2013).
[46] S. Qian, B. Das, and X. Luo, Diffusioosmotic flows in slit nanochannels, J. Colloid Interface Sci. **315**, 721 (2007).
[47] K. L. Liu, J. P. Hsu, and S. Tseng, Capillary osmosis in a charged nanopore connecting two large reservoirs, Langmuir **29**, 9598 (2013).
[48] E. Choi, K. Kwon, D. Kim, and J. Park, Lab Chip, Lab Chip **15**, 168 (2015).
[49] D. Deng, W. Aouad, W. A. Braff, S. Schlumpberger, M. E. Suss, and M. Z. Bazant, Water purification by shock electrodialysis: Deionization, filtration, separation, and disinfection, Desalination **357**, 77 (2015).
[50] R. Chein and B. Liu, Energy conversion from electrolyte concentration gradient using charged nano-pores, Int. J. Green Energy **13**, 1400 (2017).
[51] K. S. Kim, W. Ryoo, M. S. Chun, and G. Y. Chung, Simulation of enhanced power generation by reverse electrodialysis stack module in serial configuration, Desalination **318**, 79 (2013).
[52] W. Kim, J. Lee, G. Yun, G. Y. Sung, and S. J. Kim, Direct Visualization of Perm-Selective Ion Transportation, Sci. Rep. **10**, 1 (2020).
[53] W. Kim, J. Lee, G. Yun, G. Y. Sung, and S. J. Kim, Direct Visualization of Perm-Selective Ion Transportation, Sci. Rep. **10**, 1 (2020).
[54] C. Lee, C. Cottin-Bizonne, A. L. Biance, P. Joseph, L. Bocquet, and C. Ybert, Osmotic flow through fully permeable nanochannels, Phys. Rev. Lett. **112**, 1 (2014).
[55] C. Lee, C. Cottin-Bizonne, R. Fulcrand, L. Joly, and C. Ybert, Nanoscale Dynamics versus Surface Interactions: What Dictates Osmotic Transport?, J. Phys. Chem. Lett. **8**, 478 (2017).
[56] K. Sears, L. Dumée, J. Schütz, M. She, C. Huynh, S. Hawkins, M. Duke, and S. Gray, Recent developments in carbon nanotube membranes for water purification and gas separation, Materials **3**, 127 (2010).
[57] R. Das, M. E. Ali, S. B. Abd Hamid, S. Ramakrishna, and Z. Z. Chowdhury, Carbon nanotube membranes for water purification: A bright future in water desalination, Desalination **336**, 97 (2014).
[58] J. Experton, X. Wu, and C. R. Martin, From ion current to electroosmotic flow rectification in asymmetric nanopore membranes, Nanomaterials **7**, 445 (2017).

[59] Z. Siwy and A. Fuliński, Fabrication of a synthetic nanopore ion pump, Physical Review Letters **89**, 198103 (2002).

[60] Z. S. Siwy, Ion-current rectification in nanopores and nanotubes with broken symmetry, Adv. Funct. Mater. **16**, 735 (2006).

[61] A. Siria, M. L. Bocquet, and L. Bocquet, New avenues for the large-scale harvesting of blue energy, Nat. Rev. Chem. **1**, 10.1038/s41570-017-0091 (2017).

[62] R. J. Hunter, *Foundations of Colloid Science*, 2nd ed. (Oxford University Press, 2001).

[63] D. J. Griffiths, *Introduction to Electrodynamics*, 4th ed. (Pearson, Boston, MA, 2013).

[64] R. F. Probstein, *Physicochemical hydrodynamics : An Introduction* (Butterworths Publishers, 1989).

[65] N. Lakshminarayanaiah, Transport phenomena in artificial membranes., Chem. Rev. **65**, 491 (1965).

[66] Y. A. Cengel and J. M. Cimbala, *Fluid Mechanics Fundamental and Applications*, 4th ed. (McGraw-Hill Education, New York, NY, 2017).

[67] D. Burgreen and F. R. Nakache, Capillary Slits', J . Phys. Chem. **68**, 1084 (1964).

[68] J. H. Masliyah and S. Bhattacharjee, *Electrokinetic and colloid transport phenomena* (John Wiley & Sons, 2006).

[69] P. Pivonka and D. Smith, Investigation of nanoscale electrohydrodynamic transport phenomena in charged porous materials, Int. J. Numer. Methods Eng. **63**, 1975 (2005).

[70] G. Westermann-Clark and C. Christoforou, The exclusion-diffusion potential in charged porous membranes, J. Electroanal. Chem. Interfacial Electrochem. **198**, 213 (1986).

[71] S. H. Behrens and D. G. Grier, The charge of glass and silica surfaces, J. Chem. Phys. **115**, 6716 (2001), 0105149.

[72] Y. Yan, Q. Sheng, C. Wang, J. Xue, and H.-C. Chang, Energy Conversion Efficiency of Nano fluidic Batteries: Hydrodynamic Slip and Access Resistance, J. Phys. Chem. C **117**, 8050 (2013).

[73] P. B. Peters, R. V. Roij, M. Z. Bazant, and P. M. Biesheuvel, Analysis of electrolyte transport through charged nanopores, Phys. Rev. E **93**, 053108 (2016).

[74] S. Gravelle, *Nanofluidics: a theoretical and numerical investigation of fluid transport in nanochannels*, Phd thesis, University of Lyon (2015).

[75] R. B. Schoch, J. Han, and P. Renaud, Transport phenomena in nanofluidics, Rev. Mod. Phys. **80**, 839 (2008).

[76] S. Shin, J. T. Ault, P. B. Warren, and H. A. Stone, Accumulation of colloidal particles in flow junctions induced by fluid flow and diffusiophoresis, Phys. Rev. X **7**, 1 (2017).

[77] A. Ajdari and L. Bocquet, Giant amplification of interfacially driven transport by hydrodynamic slip: Diffusioosmosis and beyond, Phys. Rev. Lett. **96**, 186102 (2006).

[78] P. Sharma, J. F. Motte, F. Fournel, B. Cross, E. Charlaix, and C. Picard, A Direct Sensor to Measure Minute Liquid Flow Rates, Nano Lett. **18**, 5726 (2018).

[79] Dynamic Measurement of Nanoflows: Realization of an Optofluidic Flow Meter to the Nanoliter-per-Minute Scale, Anal. Chem. **91**, 10713 (2019).